



Published in final edited form as:

Nature. 2018 June ; 558(7711): 600–604. doi:10.1038/s41586-018-0235-7.

Altered exocrine function can drive adipose wasting in early pancreatic cancer

Laura V. Dana^{1,13}, Ana Babic^{2,13}, Michael H. Rosenthal², Emily Dennstedt¹, Alexander Muir¹, Evan C. Lien¹, Jared R. Mayers¹, Karen Tai¹, Allison N. Lau¹, Paul Jones-Sali¹, Carla M. Prado³, Gloria M. Petersen⁴, Naoki Takahashi⁴, Motokazu Sugimoto⁴, Jen Jen Yeh⁵, Nicole Lopez⁶, Nabeel Bardeesy⁷, Carlos Fernandez-del Castillo⁷, Andrew S. Liss⁷, Albert C. Koong^{8,9}, Justin Bui^{9,10}, Chen Yuan², Marisa W. Welch², Lauren K. Brais², Matthew H. Kulke^{2,11}, Courtney Dennis¹², Clary B. Clish¹², Brian M. Wolpin^{2,†}, and Matthew Vander Heiden^{1,2,12,†}

¹Koch Institute for Integrative Cancer Research and Department of Biology, Massachusetts Institute of Technology, Cambridge, MA 02139, USA

²Dana-Farber Cancer Institute, Boston, MA 02115, USA

³Department of Agricultural, Food and Nutritional Science, University of Alberta, Edmonton, Canada

⁴Mayo Clinic, Rochester, MN

⁵University of North Carolina at Chapel Hill, Chapel Hill, NC, Department of Surgery, University of North Carolina at Chapel Hill, Chapel Hill, NC

⁶University of California San Diego School of Medicine, La Jolla CA

⁷Massachusetts General Hospital Cancer Center, Harvard Medical School, Boston, MA

⁸MD Anderson, Department of Radiation Oncology, Houston, TX

⁹Stanford Cancer Institute, Stanford, CA

¹⁰David Geffen School of Medicine at University of California, Los Angeles, CA

¹¹Boston University and Boston Medical Center, Section of Hematology/Oncology, Boston, MA

Users may view, print, copy, and download text and data-mine the content in such documents, for the purposes of academic research, subject always to the full Conditions of use: http://www.nature.com/authors/editorial_policies/license.html#terms

†Correspondence: Brian Wolpin (bwolpin@partners.org) or Matthew Vander Heiden (mvh@mit.edu).

¹³Co-first authors

Author contributions

L.V.D. designed, performed, and analyzed the animal experiments with input from M.G.V.H. L.V.D., A.B., B.M.W. and M.V.G.H. wrote the manuscript with assistance from all other authors. E.D. and P.J. S. assisted with animal experimentation. A.M. immortalized and A.N.L. isolated PSCs. E.C.L. performed caloric restriction experiments. J.R.M. performed muscle volume measurements and blood measurements. K.R. performed NEFA and glycerol assays. A.B., M.H.R., C.B.C., B.M.W. designed the human study. G.M.P., N.T., M.S., J.J.Y., N.L., N.B., C.F.C., A.S.L., A.C.K., J.B., C.Y., M.W.W., L.K.B., M.H.K., B.M.W. were involved in patient recruitment and patient data collection. C.D. and C.B.C. were involved in human metabolite measurements. A.B. and M.H.R. were analyzed human data. B.M.W. supervised human study.

Competing Interests

The authors declare no competing financial interest; however, M.G.V.H. discloses serving on the S.A.B. of Agios Pharmaceuticals and Aeglea Biotherapeutics.

¹²Broad Institute of MIT and Harvard University, Cambridge, MA

Abstract

Changes in cell and organismal metabolism accompany malignancy^{1,2}. Pancreatic ductal adenocarcinoma (PDAC) is associated with peripheral tissue wasting, a metabolic syndrome that lowers quality of life and is proposed to decrease cancer patient survival^{3,4}. Tissue wasting is a multifactorial disease and targeting specific circulating factors to reverse this syndrome has been mostly ineffective in the clinic^{5,6}. Here, we show that both adipose and muscle tissue loss occur early in pancreatic cancer development. Using syngeneic PDAC mouse models, we show that tumor growth in the pancreas but not in other sites leads to adipose tissue wasting, suggesting that tumor growth within the pancreatic environment contributes to this wasting phenotype. We find decreased exocrine pancreatic function drives adipose tissue loss and pancreatic enzyme replacement attenuates PDAC-associated peripheral tissue wasting. Paradoxically, reversal of adipose tissue loss impairs survival in mice with PDAC. Upon analysis of PDAC patients, we find that adipose and skeletal muscle depletion at the time of diagnosis is not associated with worse survival. Taken together, these results provide an explanation for adipose tissue wasting in early PDAC and suggest that early peripheral tissue loss associated with pancreatic cancer may not impair survival.

Autochthonous PDAC mouse models recapitulate many features of human disease including cachexia^{7,8}. We confirmed severe adipose tissue (AT) and skeletal muscle wasting in advanced disease using two autochthonous mouse models with *Kras*^{G12D} activation and loss of *Trp53* function – either via *Trp53* deletion (KP^{-/-}C) or mutant *Trp53*^{R172H} expression (KPC) (Fig. 1a–f). Because tissue protein breakdown occurs early in PDAC⁹, we assessed tissue wasting kinetics in the KP^{-/-}C model and found decreased AT mass by 6 weeks of age, a time when pancreatic tissue weight was unchanged and plasma BCAAs, a measure of peripheral tissue wasting⁹, were modestly elevated (Fig. 1g–i, Extended Data Fig. 1a). AT wasting was greater than skeletal muscle wasting throughout disease progression (Fig. 1g–h), consistent with AT depletion preceding skeletal muscle loss^{10,11}.

Histological analysis of gastrocnemius skeletal muscle (GA) in 6-week-old KP^{-/-}C mice (early KP^{-/-}C) suggested muscle atrophy characterized by decreased myofiber cross-sectional area (Extended Data Fig. 1b–c). Using micro computed tomography (μ CT) imaging of the lower leg muscles (GA and soleus), we found decreased muscle volume in early KP^{-/-}C mice (Extended Data Fig. 1d–e). We also observed decreased muscle mass and elevated expression of genes involved in autophagy and ubiquitin-proteasome degradation, suggesting activation of muscle breakdown (Extended Data Fig. 1f–g). Histological analysis of AT also revealed smaller adipocytes and enhanced lipolysis adipocytes in early KP^{-/-}C mice (Extended Data 1h–l), suggesting reduced triglyceride synthesis or triglyceride storage. These results are consistent with enhanced lipolysis^{12,13} and muscle proteolysis¹⁴ in advanced cancer; however, in KP^{-/-}C mice these changes occur by 6 weeks of age, suggesting peripheral tissue loss is initiated early in PDAC.

Although the KP^{-/-}C model has predictable disease progression⁹, there is widespread pancreatic transformation and cancer progresses in young mice such that tissue depletion

could involve a failure to gain mass. To determine whether peripheral tissue wasting occurs in other PDAC models with longer time to disease onset, we assessed adipose and skeletal muscle mass in mice where oncogenic *Kras*^{G12D} alone is activated in the pancreas (KC). KC mice develop premalignant lesions that progress to invasive tumors with advanced age⁸. In 15-week-old KC mice, an age preceding invasive cancer, we also observe decreased adipose and skeletal muscle mass (Fig. 1j–l, Extended Data Fig. 1m). These data argue peripheral tissue wasting in PDAC is initiated early and prior to frank cancer onset.

To test whether a PDAC-derived systemic factor mediates early tissue wasting in PDAC, we implanted PDAC cells isolated from autochthonous tumors either subcutaneously or orthotopically into the pancreas of syngeneic mice (Fig. 2a). When implanted into either location, solitary tumors form with similar histological features (Fig. 2b). Although mice were injected with the same number of cells, only the mice bearing orthotopic pancreatic tumors developed marked adipose wasting (Fig. 2c–d). Subcutaneous tumors are deficient in stromal components and may display reduced desmoplasia, although similar trichrome staining is observed in subcutaneous and orthotopic tumors, suggesting similar fibrosis (Fig. 2b). We isolated and immortalized pancreatic stellate cells (PSCs) from syngeneic mice¹⁵ and injected PDAC cells alone or with PSCs to form subcutaneous or pancreatic orthotopic tumors and tested whether this major component of the stroma contributes to peripheral tissue loss. Although we found that addition of PSCs did not alter peripheral tissue wasting, tumor location still contributed to tissue wasting (Fig. 2e–f). We next examined secreted factors reported to be elevated in late-stage PDAC and/or known to induce cachexia in other models^{4,16} and found no differences between control and early *KP*^{-/-}*C* mice (Extended Data Fig. 2). These results argue tumor growth in the pancreas, rather than a known systemic circulating PDAC-derived factor, promotes early AT wasting.

To explore how tumor growth in the pancreas promotes AT wasting, we assessed systemic O₂ consumption, CO₂ production, and calculated the respiratory exchange ratio (RER). Both control and early *KP*^{-/-}*C* mice displayed similar RER (Fig. 2g), arguing against a shift in whole-body fuel source utilization. However, O₂ consumption and CO₂ production were lower in early *KP*^{-/-}*C* mice (Fig. 2h–i), suggesting decreased nutrient oxidation. Because food intake was similar between groups (Fig. 2j), early *KP*^{-/-}*C* mice may metabolize less food and altered pancreatic function could explain these findings as well as AT loss.

To assess endocrine pancreatic function, we measured plasma glucagon and insulin. While we found no significant differences in glucagon (Fig. 3a), early *KP*^{-/-}*C* mice displayed lower fed insulin (Fig. 3b). To test for an insulin secretion defect, we measured plasma insulin after a bolus glucose injection and found no significant differences (Fig. 3c). These results suggest endocrine pancreatic function is not altered in early PDAC; rather, impaired dietary absorption or starch breakdown could cause lower fed insulin levels. Consistent with this idea, we observed lower fed blood glucose levels in early *KP*^{-/-}*C* mice (Fig. 3d). Furthermore, reduced insulin levels may promote increased lipolysis and AT loss.

To assess exocrine pancreatic function, we measured fecal lipid content and found higher fecal lipids in early *KP*^{-/-}*C* mice (Fig. 3e). We also found decreased fecal protease activity and increased fecal protein content in these mice (Fig. 3f–g). Orthotopic implantation of

PDAC cells also led to increased fecal protein content during disease progression (Fig. 3h). Decreased pancreatic exocrine function could explain why early KP-/-C mice display decreased O₂ consumption and CO₂ production despite normal food intake, leading to a starvation-like response with mobilization of energy stores from peripheral tissues. Indeed, mice bearing subcutaneous PDAC tumors fed a calorically restricted diet displayed enhanced AT loss compared to skeletal muscle loss and reduced tumor size (Extended Data Fig. 3a-d).

To test whether decreased exocrine pancreatic function contributes to tissue wasting in PDAC, we supplemented a diet with pancreatic enzymes (Fig. 3i). Providing pancreatic enzymes attenuated adipose wasting in PDAC mice (Fig. 3j). Furthermore, while early PDAC mice displayed decreased fed glucose levels (Fig. 3d), pancreatic enzyme supplemented PDAC mice displayed similar glucose levels to control littermates (Extended Data Fig. 3e). To control for potential food intake differences associated with adding pancreatic enzymes to a diet, we pair fed mice to assure similar food consumption, and again observed attenuated AT loss in PDAC when providing pancreatic enzymes (Extended Data Fig. 3f-i). These results confirm decreased pancreatic exocrine function mediates AT loss and contributes to peripheral tissue wasting in mice with early PDAC.

Cachexia has been proposed to worsen patient survival in various cancers including PDAC^{3,4}. To determine whether AT wasting limits survival in PDAC, we assessed whether pancreatic enzyme supplementation improved disease outcome. Surprisingly, despite reduced AT wasting, pancreatic enzyme supplementation decreased PDAC mouse survival (Fig. 3k), suggesting peripheral tissue wasting may not always limit survival.

To investigate the association of peripheral tissue wasting and patient survival, we identified 782 patients at five U.S. cancer centers with previously untreated PDAC, available clinical and outcome data, and banked blood samples (Extended Data Table 1). We quantified lumbar visceral and subcutaneous AT areas using pretreatment CT scans (Extended Data Fig. S4a)^{17,18}. Although AT area was associated with multiple clinical factors (Extended Data Table 2), no association was found between AT wasting and patient survival in the full population (Table 1) or by disease stage (Extended Data Table 3a).

Studies of muscle wasting and PDAC patient survival have led to conflicting results^{17,19-22}, potentially due to differences in study design. We next used CT imaging to measure lumbar skeletal muscle index (SMI), a marker of muscle mass^{17,19,20,22}. Using established cut-points for sarcopenia¹⁴, we found that 65% of patients displayed sarcopenia at diagnosis, and these patients did not have worse survival (Table 1). Interestingly, the prevalence of sarcopenia was not different by disease stage (localized, 64%; locally advanced, 70%; and metastatic disease, 63%; $P=0.40$). Since an interaction between sarcopenia and BMI was proposed^{20,22}, we evaluated whether sarcopenic obesity was associated with worse patient survival and observed no survival differences (Table 1). Because optimal sarcopenia cut-points are not well defined¹⁴, we investigated an agnostic SMI classification into gender-specific quintiles and found no association with patient survival (Extended Data Table 3b). We also examined muscle area and attenuation and did not identify an association of these markers with patient survival (Extended Data Table 3b). Finally, because plasma BCAAs

elevations reflect tissue wasting in early PDAC⁹, we evaluated whether plasma BCAAs at diagnosis were associated with reduced survival and did not identify worse outcomes with elevated BCAAs (Extended Data Tables 4–6, Extended Data Fig. 4b). Thus, in this multi-institutional patient population with newly diagnosed, previously-untreated PDAC, we found no evidence that early skeletal muscle or AT wasting was associated with worse survival.

Independent of effects on survival, assessing peripheral tissue loss before overt disease onset may help identify PDAC at earlier stages. In mouse models, we found decreased exocrine function contributes to AT wasting. Many PDAC patients experience loss of exocrine pancreatic function²³; however, whether decreased exocrine function contributes to wasting in patients requires further study. Furthermore, correction of pancreatic exocrine function in mouse models reduces AT wasting but does not significantly affect muscle loss, suggesting that pancreatic enzyme supplementation is either insufficient to fully restore the nutritional state or additional factors contribute to muscle wasting. These other factors may include stroma-derived inflammatory signals that were not tested in this study. Nevertheless, the findings that a starvation-like state in PDAC mouse models contributes to AT loss and increases survival are in agreement with data suggesting caloric restriction improves PDAC survival²⁴, perhaps via similar mechanisms. Although not examined here, changes in insulin levels may contribute to survival differences upon reversal of a starvation-like state. The finding that pancreatic enzyme supplementation led to worse survival in mice, also suggests peripheral tissue wasting in early PDAC may be distinct from cachexia associated with late-stage disease. Nutritional intervention and pancreatic enzyme replacement are sometimes used in PDAC patients²⁵ and better understanding the mechanisms that cause tissue wasting across cancer types and stages of disease is needed to design interventions that reduce functional disability and improve survival in cancer patients.

Methods

Cell culture

All cells were cultured in DMEM supplemented with 10% FBS (Corning) and 1% penicillin and streptomycin (Corning).

Western blot analysis

Antibodies recognizing pHSL (Ser563) (#4139) and total HSL (#4107) were purchased from Cell Signaling Technologies.

Animal studies

All experiments performed in this study were approved by the MIT Committee on Animal Care (IACUC). Furthermore, for subcutaneous tumor growth, a maximum tumor burden of 2 cm³ was permitted by our IACUC protocol and these limits were not exceeded. All mice in this study were fully backcrossed to the C57Bl/6J background, and housed on a 12-hour light and 12-hour dark cycle, and co-housed with littermates with ad lib access to water and food, unless otherwise stated. Furthermore, all experimental groups were age-matched and assigned based on genotype (or treatment). All animals were numbered and experiments conducted in a blinded manner. After data collection, genotypes were revealed and animals

assigned to groups for analysis. All measurements were collected from distinct animals, n represents biologically independent samples, and mice were analyzed as tumors were developed. Furthermore, no statistical methods were performed to predetermine sample size.

For studies utilizing $Kras^{G12D};Trp53^{fl/fl};Pdx1\text{-cre}$ (KP $^{-/-}$ C) mice, controls included littermate mice that lacked the cre-recombinase allele, LSL- $Kras^{G12D}$ allele, or both. For studies utilizing $Kras^{G12D};Trp53^{R172H/+};Pdx1\text{-cre}$ (KPC) mice, control mice included littermates that lacked the LSL- $Kras^{G12D}$ allele or LSL- $P53^{172H}$ allele. For studies utilizing $Kras^{G12D};Pdx1\text{-cre}$ (KC) mice, control mice included littermates expressing the cre allele.

For subcutaneous or pancreatic orthotopic tumors, C57Bl/6J mice (000664) were injected with 10^5 murine PDAC cells isolated from C57Bl/6J KP $^{-/-}$ C mice as previously described⁹. Phosphate-buffered saline (PBS) or PDAC-cells were injected into the right flank (in 100 μ L) or the pancreas of 8wk old C57Bl/6J mice (50 μ L). For protein fecal collection studies in mice bearing orthotopic pancreatic tumors, mice were injected with 10^5 murine PDAC cells (50 μ L) and allowed to recover from surgery for 2 weeks. Fecal matter was collected after this 2 week recovery time every 2–3 days for approximately 2–3 weeks and placed in -20°C until day of analysis. For studies utilizing pancreatic stellate cells (PSCs), we isolated PSCs as previously described²⁶. After a few passages, PSCs were immortalized and injected at a 1:1 ratio as previously described.¹⁵

For experiments using metabolic cages, 5–6wk old mice were placed in metabolic cages and food intake, RER, volumetric rate of O_2 consumption, and volumetric of CO_2 production were measured over a 3-day period (TSE systems). RER was calculated using the following formula $\text{RER} = \text{VCO}_2/\text{VO}_2$.

For pair-feeding experiments, the amount of diet supplemented with pancreatic enzymes that was consumed per mouse per day was calculated for an average of 5 days. Animals with early PDAC were weighed, individually housed, and randomly given a pre-weighed quantity of food that was either control diet or diet supplemented with pancreatic enzymes. Mice were weighed prior to the start of the food-pairing experiment to ensure both groups of mice had similar starting body weights.

For caloric restriction studies, mice were injected subcutaneously (into both flanks) with PDAC-derived cells as described above. Animals were randomly placed on AIN-93G (TD.94045) control diet and or same diet at 40% restriction after tumors were palpable. Mice were individually housed and fed daily either 3.2 g/day (control mice) or 1.9 g/day (calorically restricted mice) for a total of 3 weeks.

Animal diets

For diets supplemented with pancreatic enzymes, AIN-93G powdered diet (TD.94045) was purchased from Envigo and mixed with a commercial preparation of pancreatic enzymes as previously described²⁷.

Assessment of glucose metabolism

Glucose levels were measured using a Breeze-2 glucose meter (Bayer). For insulin measurements, we used an Ultra Sensitive Mouse insulin ELISA (#90080) following the manufacturer's protocol. For *in vivo* insulin secretion, mice were fasted for 16h and i.p. injected with glucose (1g/kg), blood samples collected and analyzed at the indicated time points.

Ex vivo lipolysis

Ex vivo lipolysis assays of adipose explants were performed as previously described²⁸. Briefly, epididymal adipose tissues were collected and incubated at 37°C, non-esterified fatty acids (NEFA) were measured using Wako diagnostics and glycerol release was measured using Sigma Free Glycerol Determination kit (FG0100) according to manufacturer's instructions.

Hormone and metabolite measurements

Blood samples were collected in EDTA-containing tubes and centrifuged 3,000 rpm for 15 minutes (4°C). Circulating levels of IL-6 (M6000B, R&D systems), corticosterone (80556, Crystal Chem), amylin (EIAM-AMY-1, RayBiotech) were measured according to the manufacturer's instructions. TNF- α , IFN γ , IL-10, IL-1 β , IL-17, IL-4 were measured using Discovery Assay (Eve Technologies). Circulating BCAAs levels were measured as previously described⁹.

μ CT animal imaging

All animal CT measurements were performed using GE eXplore CT120. The scans were conducted at 70kVp, 50mA, and 32ms. There were 720 views, 0.5 degrees apart over a full 360-degree rotation. To assess muscle volume, a 3D Gaussian filter was used in an area extending from the right ankle to the proximal end of the fibula. This filtered data set was used to determine areas corresponding to leg muscle while excluding other tissues. This was done in Matlab using connected components (bwconncomp) function. Having created the mask (segmented the leg muscle from other tissues), a histogram of the muscle region was calculated. Voxels falling within the density range 160–200 Hounsfield units (HU) were considered muscle. This was done to correct for any overlap of the muscle mask with adjacent bone or adipose (higher and lower HU values respectively).

Fecal assays

To assess total fecal protein, 10mg of feces were re-suspended in lysis buffer (2% SDS, 150mM NaCl, .5M EDTA), sonicated, and protein concentration assessed using BCA assay according to manufacturer's instructions. Total fecal protease activity was measured as previously described²⁹. Briefly, 10–30 mg of fecal matter was resuspended in 1mL of buffer A (.1% Triton X-100, .5M NaCl, 100 mM CaCl₂), sonicated, and centrifuged. The supernatant was then incubated with 3% Azo-Casein (Sigma A2765) 37°C for 60 min. The reaction was stopped using 8% trichloroacetic acid and centrifuged. The absorbance of the supernatant (366 nm) was measured using a spectrophotometer. Total fecal lipids were measured as previously described³⁰. Briefly, 1,000 mg of feces were collected and lipids

extracted using 2:1 Chloroform to Methanol. The lipid fraction was dried using a stream of gaseous nitrogen and vials weighed.

Histological Analysis

Tissues were fixed overnight with neutral-buffered 10% formalin, paraffin embedded, sectioned, and stained with hematoxylin and eosin or stained with Masson's Trichrome using standard protocols.

Statistics for animal data

All data is presented was graphed using Prism (GraphPad) software and depicted as mean \pm SEM. Unless otherwise indicated, *P* values were determined using unpaired two-sided *t*-test. Statistical outliers were measured using Grubb's outlier test (Prism) and excluded from final analysis.

Human population study

Study population—Our study population included pancreatic cancer patients from five U.S. cancer centers: Dana-Farber/Brigham and Women's Cancer Center (DF/BWCC), Massachusetts General Hospital (MGH), Mayo Clinic, Stanford University, and University of North Carolina-Chapel Hill (UNC). We included 782 patients with pancreatic adenocarcinoma who were diagnosed between 2000 and 2015, and had a stored plasma sample collected prior to receiving any treatment for their malignancy, including surgery, radiation or chemotherapy. A total of 778 patients at the five institutions met these criteria and had a plasma sample collected within 30 days before their pathological diagnosis and 60 days after this diagnosis. Of these patients, 687 had an available computed tomography (CT) scan performed during this time period for analysis of body composition. The overall study was approved by the Dana-Farber/Harvard Cancer Center IRB, and data abstraction and blood sample collection was approved by each individual institutional IRB. All participants provided informed consent.

Human plasma samples and metabolite profiling

Blood was collected in sterile EDTA tubes, and processed within 3 hours (DFCI, Mayo Clinic, Stanford University, UNC) or 24 hours (MGH) for separation into plasma and other components. Plasma was aliquoted into cryovials and stored at -80° C. Plasma samples were thawed once on wet ice to aliquot into smaller sample volumes for analysis, de-identified, and sent for analysis in a single shipment.

Liquid chromatography tandem mass spectrometry (LC-MS) analyses were conducted using a Shimadzu Nexera X2 U-HPLC (Shimadzu Corp.; Marlborough, MA) coupled to a Q Exactive hybrid quadrupole orbitrap mass spectrometer (Thermo Fisher Scientific; Waltham, MA). Polar metabolites were extracted from plasma (10 μ L) using 90 μ L of 74.9:24.9:0.2 v/v/v acetonitrile/methanol/formic acid containing stable isotope-labeled internal standards (valine-d8, Sigma-Aldrich; St. Louis, MO; and phenylalanine-d8, Cambridge Isotope Laboratories; Andover, MA). The samples were centrifuged (10 min, $9,000 \times g$, 4° C), and the supernatants were injected directly onto a 150×2 mm, 3 μ m Atlantis HILIC column (Waters; Milford, MA). The column was eluted isocratically at a flow rate of 250 μ L/min

with 5% mobile phase A (10 mM ammonium formate and 0.1% formic acid in water) for 0.5 minute followed by a linear gradient to 40% mobile phase B (acetonitrile with 0.1% formic acid) over 10 minutes. MS analyses were carried out using electrospray ionization in the positive ion mode using full scan analysis over 70–800 m/z at 70,000 resolution and 3 Hz data acquisition rate. Other MS settings were: sheath gas 40, sweep gas 2, spray voltage 3.5 kV, capillary temperature 350°C, S-lens RF 40, heater temperature 300°C, microscans 1, automatic gain control target 1e6, and maximum ion time 250 ms. Raw data were processed using TraceFinder software (Thermo Fisher Scientific; Waltham, MA). Metabolite identities were confirmed using authentic reference standards.

To evaluate reproducibility of BCAA measurements, we included 77 blinded quality control (QC) plasma samples within the larger sample set, from eight plasma QC pools. The mean coefficients of variance were 7.6% for isoleucine, 8.0% for leucine, and 7.3% for valine. Since blood samples from MGH were processed after >3 hours, we evaluated the reproducibility of BCAA measurements between samples processed at different time points after collection. For 10 patients, we processed blood immediately and at 24 hours and measured plasma BCAAs. Spearman correlation coefficients for the BCAA levels at the two time points were 0.95 for isoleucine, 0.95 for leucine, and 0.92 for valine. All blood samples were collected into EDTA plasma tubes, except for 28 blood samples collected as serum from MGH patients. To evaluate BCAAs in plasma versus serum tubes, we measured BCAA levels among 10 patients who had simultaneous collection of plasma and serum. Spearman correlation coefficients for plasma BCAAs by plasma versus serum samples were 0.84 for isoleucine, 0.76 for leucine, and 0.94 for valine. Given the high correlation coefficients for plasma BCAAs by both time of blood processing and plasma versus serum collection, we included all MGH patients in our study population.

Computed tomography imaging quantitation of muscle and adipose tissue in patients

Muscle, visceral adipose tissue, and subcutaneous adipose tissue areas were measured through the third lumbar vertebra landmark on CT imaging as previously published^{17,18}. Scans from the DF/BWCC, MGH, Stanford University, and UNC study sites (n=363) were manually segmented using Slice-O-Matic software (v4.3; Tomovision, Montreal, Canada) by trained image analysts with final verification from a board-certified radiologist. All paraspinal and abdominal wall muscles were included in the muscle area. The Hounsfield CT attenuation scale was used to constrain adipose tissue and muscle selection. The Hounsfield scale is a linear transformation of the linear attenuation coefficient, with fixed points calibrated for air at –1000 Hounsfield units (HU) and water at 0 HU. All medical CT scanners are routinely calibrated to this scale. Pixel attenuation constraints of –29 to +150 HU were used for muscle and –180 to –30 HU for adipose tissue as previously published^{17,18}. The visceral adipose tissue compartment was defined by the peritoneum; all extraperitoneal adipose tissue was included in the subcutaneous compartment. Pixel dimensions were extracted from scanner parameters embedded within the scan data; total area was measured as the product of segmented pixel count and pixel area. We calculated skeletal muscle index (SMI) as the ratio of skeletal muscle area (cm²) to height squared (m²). Muscle attenuation was defined as the average Hounsfield attenuation of all pixels in

the muscle area. Analyst performance was tested, and a test-retest coefficient of variation < 1.1% was observed for all analysts and parameters.

Scans from the Mayo Clinic site (n=324) were analyzed using in-house developed software written in Matlab (Matlab 2015b, MathWorks, Natick, MA) with manual correction by a trained image analyst. The software automatically fits three concentric closed contours at the air-skin boundary, the subcutaneous adipose-muscle boundary, and the abdominal wall-peritoneal adipose boundary using hierarchical morphological classification constrained by a prior probability shape model. These boundaries defined the same zones as were described for the Slice-O-Matic method. The software also automatically created masks for bone and colonic content and these masks were used to exclude bone and colonic content from being included as muscle or adipose tissue. The final boundaries were verified by a board-certified radiologist. Adipose and muscle areas were then calculated for each compartment using the same attenuation constraints as described for the Slice-O-Matic method

To ensure consistency across sites, we analyzed 20 cases using both methods and found a coefficient of variation of 2.4%, 1.7%, and 3.8% between the methods for the skeletal muscle, subcutaneous adipose tissue, and visceral adipose tissue areas respectively. The maximum observed differences were 4.1%, 3.6%, and 15.2% for these compartments.

Covariate Data and Statistical Analysis of Patient Data

Using patient questionnaires and medical records, we extracted information on patient and clinical characteristics, including: age at diagnosis, gender, race/ethnicity, height, weight at blood collection, diabetes history (no diabetes, diabetes of duration <4 years, diabetes of duration ≥ 4 years), tobacco use (never, past, current), primary tumor location (head or uncinate, body, tail, other), cancer stage (local, locally advanced, metastatic), year of diagnosis, and survival time.

Body composition measurements and plasma BCAAs by patient characteristics were compared using Wilcoxon rank-sum test or Kruskal-Wallis test. Pearson correlation test was used to evaluate the linear relationship between body composition measurements, plasma BCAAs and other patient characteristics. To evaluate the associations between patient survival, body composition measurements, and plasma BCAAs, we used multivariable-adjusted Cox proportional hazards regression and calculated hazard ratios (HRs) and 95% confidence intervals (CI). Survival time was calculated as the time from diagnosis to death or date of last follow-up if the patient was still alive. In an initial multivariate model, we adjusted for age at diagnosis (continuous), gender (male, female), race (White, non-White, unknown), year of diagnosis (2000–2005, 2006–2010, 2011–2015), institution (DF/BWCC, MGH, Mayo Clinic, Stanford University, UNC), and cancer stage (localized, locally advanced, metastatic, unknown). In a second multivariate model, we additionally adjusted for BMI (continuous), history of diabetes (none, <4yrs, >4yrs, unknown), and smoking status (never, past, current, unknown), which have previously been shown to associate with patient survival^{31,32}.

Since cut-offs to define clinically relevant body composition categories are not well defined, we also divided patients into quintiles by AT and muscle tissue measurements. Since

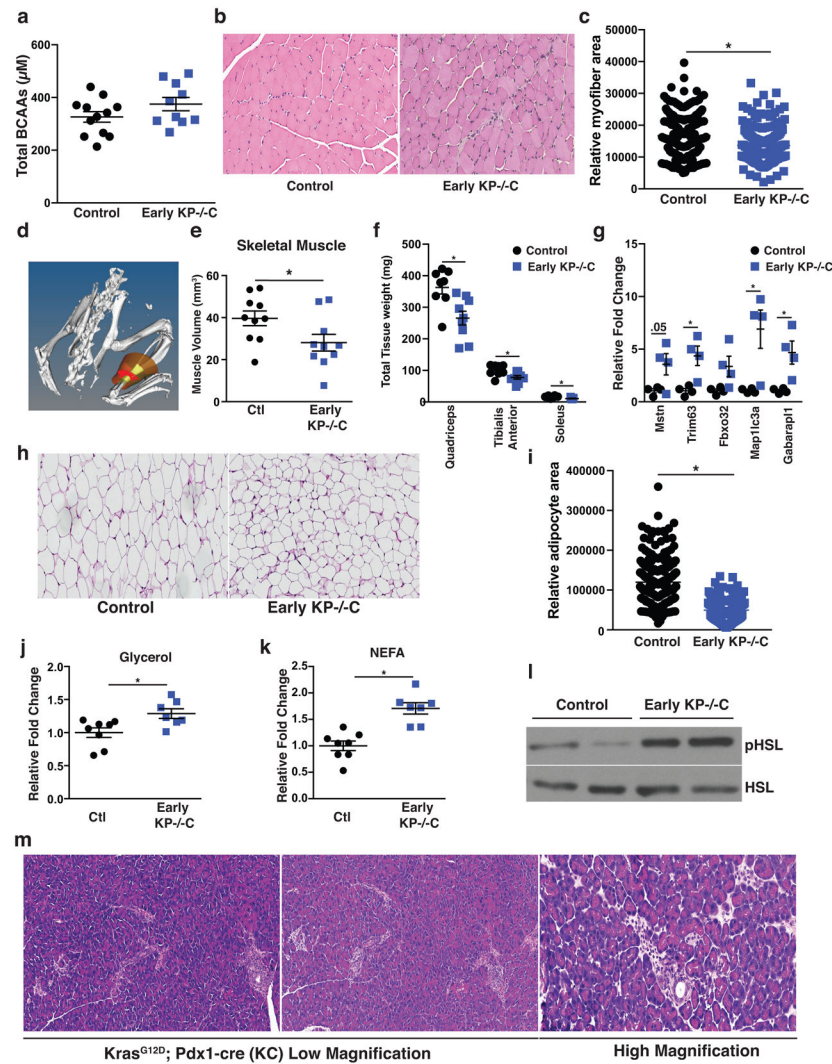
distribution of body composition measurements differed by gender (Supplementary Table 2), we created gender-specific quintiles for all body composition measurements. *P*-values for linear trend were calculated by entering the quantile-specific median value for body composition measurements in the Cox proportional hazards models.

To evaluate sarcopenia, we used the SMI criteria established by a recent international consensus definition of cancer cachexia¹⁴. The SMI cut-offs were 55.4 cm²/m² for men, and 38.9 cm²/m² for women. To evaluate sarcopenic obesity, we generated a combined variable, where overweight/obesity status is defined as BMI ≥ 25kg/m², similar to a previous study in patients with PDAC²². The resulting four categories were overweight/obese and sarcopenic, overweight/obese and non-sarcopenic, non-overweight/obese and sarcopenic, non-overweight/obese and non-sarcopenic. For plasma BCAAs, patients were divided into quartiles, with quartiles 2–4 compared to quartile 1 as the referent. *P*-value for trend was calculated by entering quartile-specific median values for total plasma BCAAs as a continuous variable in the Cox proportional hazards model.

We performed stratified analyses by disease stage, and statistical interaction was assessed by the Wald test of the cross-product term between stage (localized, locally advanced, metastatic, unknown) and tissue measurements (continuous). We also calculated the HR for each institution and measured heterogeneity across centers using the Cochran's Q statistic³³. This statistic is a weighted sum of squared deviations of an individual study's estimate from the overall estimate obtained by meta-analysis. All analyses were performed with SAS 9.2 statistical analysis software, and all *P*-values were two-sided.

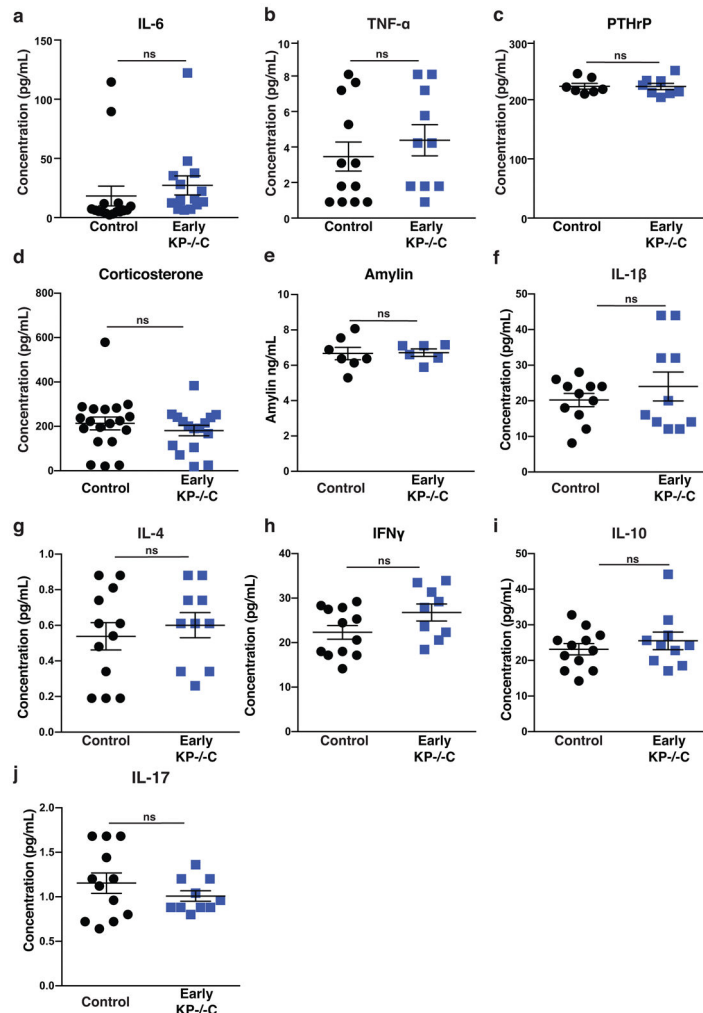
Data Availability—Source data for the graphical representations found in all figures (Fig 1–3) and Extended Data figures (Fig. S1–S3) have been provided. All other data that supports the findings of this study are available upon request.

Extended Data



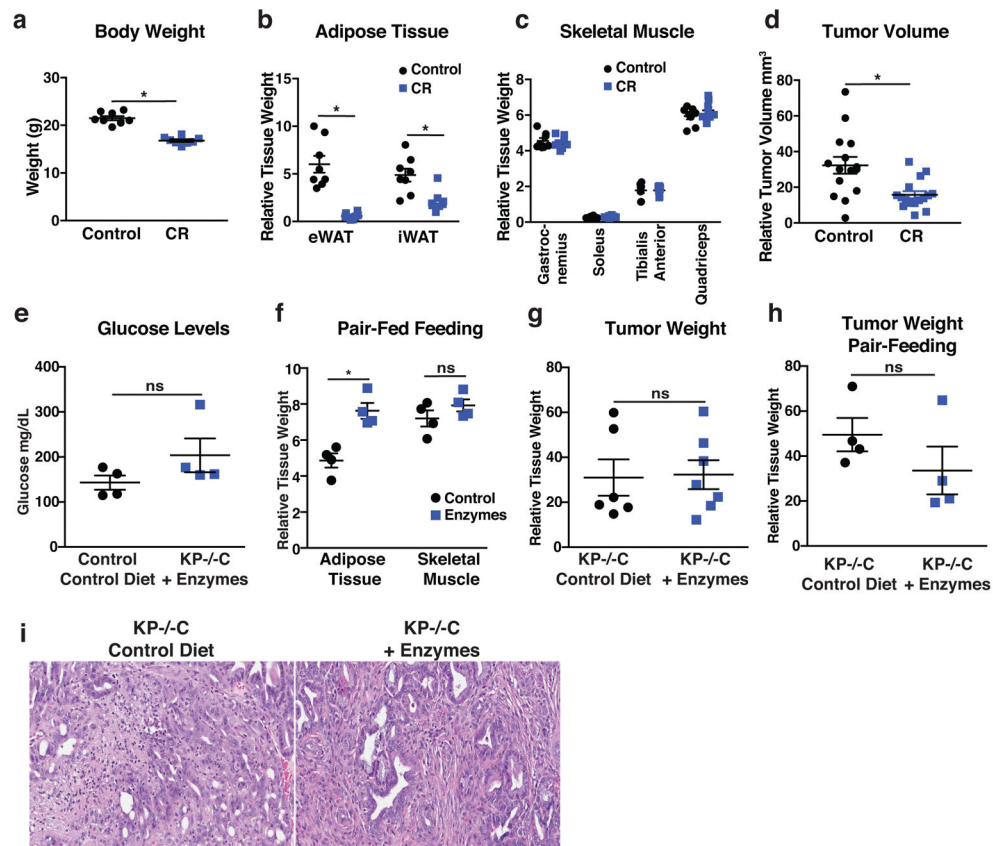
Extended Data Figure 1. PDAC is associated with adipose and skeletal muscle wasting
a. Circulating BCAAs (μM) (Valine, Leucine, and Isoleucine) in male control and early KP $^{-/-}$ C mice ($N=12, 10$). **b.** Representative histology of H&E stained gastrocnemius muscle (GA) of early KP $^{-/-}$ C mice ($N=4$). **c.** Relative myofiber area in male control and early KP $^{-/-}$ C mice ($N=3$) ($P<.0001$). **d.** Representative 3D μCT imaging reconstruction of soleus and gastrocnemius skeletal muscle (highlighted in red). **e.** Relative soleus and gastrocnemius skeletal muscle as assessed by μCT scan of control and early KP $^{-/-}$ C male mice ($N=10$) ($P=.04$). **f.** Skeletal muscle tissue mass of the indicated muscle groups in male control and early KP $^{-/-}$ C mice ($N=8, 9$) ($P=.006$ (Quadriceps), $P=.02$ (Tibialis Anterior), $P=.004$ (Soleus)). **g.** Relative mRNA expression of the indicated genes assessed by RT-qPCR ($N=4$) ($P=.05$ (Mstn), $P=.01$ (Trim63), $P=.07$ (Fbxo32), $P=.00004$ (Map1lc3a), $P=.006$ (Gabarapl1)). **h.** Representative histology of H&E stained epididymal adipose tissue from control and early KP $^{-/-}$ C male mice ($N=4$). **i.** Relative adipocyte area in male control and early KP $^{-/-}$ C mice ($N=3$) ($P<.0001$). **j.** Glycerol release in *ex vivo* adipose tissue explants

from control and early KP^{-/-}C male mice (N=7) ($P= .01$). **k.** Non-esterified fatty acid (NEFA) release in *ex vivo* adipose tissue explants from control and KP^{-/-}C male mice (N=8, 7) ($P=0.002$). **l.** Representative western blot analysis of pHSL and HSL expression in adipose tissue of control and early KP^{-/-}C male mice (N=3). **m.** Representative H&E histology of pancreata in 15wk KC male mice (N=5). Unless otherwise indicated, statistical analysis was performed using unpaired two-sided *t*-test, data are mean \pm SEM, and N represents number of mice analyzed.



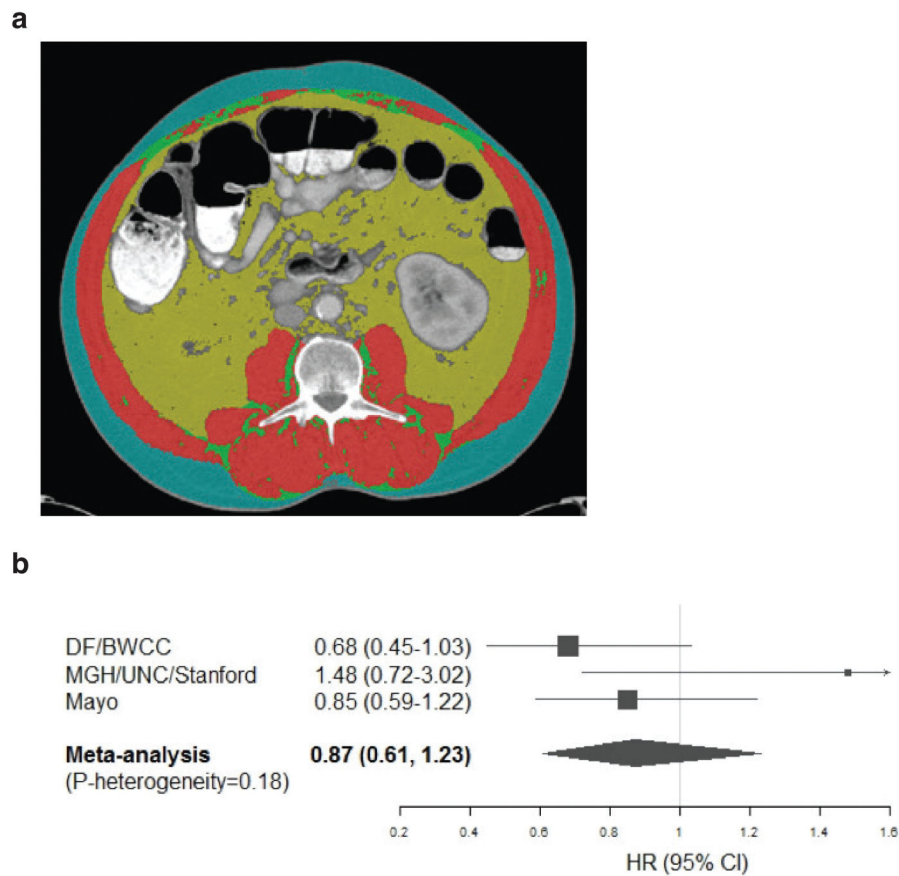
Extended Data Figure 2. Systemic circulating factors are not altered in early PDAC

a–j Circulating levels of the indicated factors in control and Early KP^{-/-}C mice. **a.** IL-6 (N=16, 14) ($P=.45$). **b.** TNF- α (N=12, 10) ($P=.45$). **c.** PTHrP (N=7, 8) ($P=.94$). **d.** Corticosterone (N=19, 16) ($P=.40$). **e.** Amylin (N=7, 6) ($P=.91$). **f.** IL-1 β (N=11, 10) ($P=.39$). **g.** IL-4 (N=12, 10) ($P=.56$). **h.** IFN γ (N=12, 9) ($P=.08$). **i.** IL-10 (N=12, 10) ($P=.42$). **j.** IL-17 (N=12, 10) ($P=.29$). Unless otherwise indicated, statistical analysis was performed using unpaired two-sided *t*-test, data are mean \pm SEM, and N represents number of mice analyzed.



Extended Data Figure 3. Decreased exocrine pancreatic function in early PDAC disease promotes adipose tissue loss

a–d. C57Bl/6J mice bearing PDAC-derived subcutaneous tumors fed a control diet or same diet at 40% caloric restriction (CR) for 3 weeks (N=8). **a.** Body weight ($P < .0001$). **b.** Epididymal adipose tissue (eWAT) and inguinal adipose tissue (iWAT) mass normalized to body weight ($P < .0001$ for eWAT and $P = .0034$ for iWAT). **c.** Skeletal muscle mass of the indicated muscle groups normalized to body weight. **d.** Tumor volume normalized to body weight ($P = .002$) (N=15 tumor (2 tumors per mouse)). **e.** Fed plasma glucose levels in 7-week-old male control and KP-/-C mice fed indicated diets (N=4) ($P = .18$). **f.** Tissue weights normalized to body weight in KP-/-C mice pair-fed indicated diets (N=4) ($P = .01$ and $P = .53$). **g–h.** Tumor weight normalized to body weight in KP-/-C mice fed indicated diets for 1wk. **g.** KP-/-C mice fed indicated diets (N=6, 7) ($P = .9$). **h.** KP-/-C mice pair-fed indicated diets (N=4) ($P = .26$). **i.** Representative histology of H&E stained autochthonous pancreatic tumors of KP-/-C mice fed indicated diets (N=4). Unless otherwise indicated, statistical analysis was performed using unpaired two-sided *t*-test, data are mean \pm SEM, and N represents number of mice analyzed.



Extended Data Figure 4. Use of CT imaging to assess patient body composition and relationship between plasma BCAAs levels and patient survival by study site

a. Representative CT image used to analyze body composition. Skeletal muscle is shown in red, intramuscular adipose tissue is shown in green, visceral adipose tissue is shown in yellow, and subcutaneous adipose tissue is shown in blue. **b.** Hazard ratios (HRs) and 95% confidence intervals (CI) for the association between plasma BCAAs and patient survival, comparing the top to bottom quartile, calculated using Cox proportional hazards model adjusted for age at diagnosis (continuous), gender (male/female), race (white, non-white, unknown), year of diagnosis (2000–2005, 2006–2010, 2011–2015), cancer stage (local, locally advanced, metastatic, unknown), BMI (continuous), diabetes history (none, 4yrs, >4yrs, unknown), and smoking status (never, past, current, unknown). The pooled HR was calculated by the DerSimonian and Laird random-effects model. The solid squares and horizontal lines correspond to the study site-specific multivariate HR and 95% CI, respectively. The area of the solid square reflects the study site-specific weight (inverse of the variance). The filled diamond represents the pooled HR and 95% CI. The solid vertical line indicates an HR of 1.0. (N=778). Abbreviations: DF/BWCC, Dana-Farber/Brigham and Women’s Cancer Center; MGH, Massachusetts General Hospital; UNC, University of North Carolina; BMI, body mass index.

Extended Data Table 1

Pancreatic cancer patient characteristics by (a) study site and (b) availability of blood samples and CT images

a.

	Overall	DF/BWCC	MGH	Stanford	UNC	Mayo
No. of patients	782	281	58	36	57	350
Diagnosis period, years						
2000–2005	110 (14)	25 (9)	0 (0)	14 (39)	0 (0)	71 (20)
2006–2010	292 (37)	90 (32)	18 (31)	15 (42)	24 (42)	145 (41)
2011–2015	380 (49)	166 (59)	40 (69)	7 (19)	33 (58)	134 (38)
Age at diagnosis, years	66.0 (10.7)	64.3 (10.0)	69.4 (10.2)	67.9 (13.1)	68.2 (11.1)	66.2 (10.7)
Female sex	347 (44)	133 (48)	28 (48)	11 (32)	31 (54)	144 (41)
White race	698 (89)	252 (90)	39 (67)	24 (67)	39 (68)	344 (98)
Body mass index, kg/m ²	27.4 (5.2)	26.7 (5.2)	27.0 (5.7)	24.7 (4.7)	27.4 (4.7)	28.2 (5.0)
Diabetes history						
No diabetes	565 (72)	194 (69)	46 (79)	28 (78)	32 (56)	265 (76)
Diabetes 4 years	100 (13)	38 (14)	5 (9)	4 (11)	8 (14)	45 (13)
Diabetes >4 years	54 (7)	20 (7)	4 (7)	2 (6)	7 (12)	21 (6)
Unknown	63 (8)	29 (10)	3 (5)	2 (6)	10 (18)	19 (5)
Tobacco use						
Never	335 (43)	127 (45)	14 (24)	18 (50)	20 (35)	156 (45)
Past	330 (42)	121 (43)	36 (62)	13 (36)	25 (44)	135 (39)
Current	68 (9)	30 (11)	8 (14)	4 (11)	12 (21)	14 (4)
Missing	49 (6)	3 (1)	0 (0)	1 (3)	0 (0)	45 (13)
Primary tumor location						
Head/Uncinate	481 (62)	161 (57)	41 (71)	24 (67)	49 (86)	206 (59)
Body	142 (18)	64 (23)	6 (10)	8 (22)	3 (5)	61 (17)
Tail	97 (12)	47 (17)	11 (19)	3 (8)	5 (9)	31 (9)
Body and tail	31 (4)	5 (2)	0 (0)	1 (3)	0 (0)	25 (7)
Head and body	22 (3)	0 (0)	0 (0)	0 (0)	0 (0)	22 (6)
Other	9 (1)	4 (1)	0 (0)	0 (0)	0 (0)	5 (1)
Cancer stage						
Local	258 (33)	52 (19)	51 (88)	5 (14)	54 (95)	96 (27)
Locally advanced	157 (20)	47 (17)	0 (0)	21 (58)	1 (2)	88 (25)
Metastatic	308 (39)	175 (62)	4 (7)	9 (25)	2 (4)	118 (34)
Unknown	59 (8)	7 (2)	3 (5)	1 (3)	0 (0)	48 (14)
Median survival, months						
Local	20.6	20.5	25.8	6.3	17.4	22.4
Locally advanced	11.0	13.0	n/a	7.9	1.4	11.1
Metastatic	7.0	6.9	15.5	4.9	3.9	8.2

b.

	Full Study Population (Pt No.)	Blood Samples (Pt No.)	CT Images (Pt No.)
DF/BWCC	281	280	244
MGH	58	58	38
Stanford	36	34	33
UNC	57	56	48
Mayo Clinic	350	350	324
Total	782	778	687

a. Continuous variables are reported as mean (standard deviation), and categorical variables are reported as number (percent) at time of diagnosis unless otherwise noted.

Abbreviations: CT, computed tomography; DF/BWCC, Dana-Farber/Brigham and Women's Cancer Center; MGH, Massachusetts General Hospital; UNC, University of North Carolina

Extended Data Table 2

Pancreatic cancer patient characteristics by body composition measurements.

	PtNo.	SMI (cm ² /m ²)	Muscle area (cm ²)	Muscle attenuation (HU)	Subcutaneous fat area (cm ²)	Visceral fat area (cm ²)
Age						
< 60 yrs	194	47.9 (9.9)	144.4 (37.4)	39.1 (9.4)	206.9 (116.6)	155.0 (107.9)
60 – <70 yrs	238	46.6 (11.1)	134.2 (34.9)	36.9 (9.6)	214.7 (115.1)	163.2 (103.5)
70 yrs	255	41.7 (7.7)	118.4 (28.9)	32.4 (9.4)	185.3 (94.2)	163.7 (111.0)
<i>P</i> -value *		9.8×10 ⁻¹³	3.3×10 ⁻¹⁴	3.0×10 ⁻¹²	0.03	0.53
Gender						
Male	384	49.5 (8.8)	153.8 (27.6)	37.0 (9.4)	185.8 (102.2)	203.0 (111.9)
Female	303	39.5 (8.5)	102.6 (17.8)	34.5 (10.3)	221.5 (113.8)	107.8 (72.7)
<i>P</i> -value *		3.7×10 ⁻⁵¹	6.5×10 ⁻⁸⁸	0.004	2.3×10 ⁻⁶	2.1×10 ⁻³¹
Race						
White	621	45.0 (10.0)	131.4 (34.4)	35.6 (9.8)	201.2 (105.5)	163.9 (105.5)
Non-White	42	46.8 (11.1)	129.7 (39.8)	37.6 (10.7)	216.4 (137.3)	117.6 (118.3)
<i>P</i> -value *		0.24	0.60	0.15	0.80	0.001
Diabetes						
No diabetes	498	44.4 (9.4)	129.4 (35.1)	37.0 (9.7)	191.4 (99.6)	148.8 (105.6)
Diabetes 4 yrs	92	45.8 (8.5)	133.5 (33.0)	33.3 (10.1)	224.4 (112.3)	189.2 (99.0)
Diabetes >4 yrs	48	48.0 (10.6)	144.1 (35.9)	35.1 (8.7)	216.5 (130.4)	207.2 (116.1)
<i>P</i> -value *		0.01	0.01	0.004	0.03	3.2×10 ⁻⁶
BMI, kg/m²						
<18.5	14	35.1 (4.6)	92.4 (15.0)	44.9 (12.2)	61.3 (51.9)	24.3 (20.7)
18.5–24.9	220	41.0 (8.0)	117.8 (31.2)	39.0 (9.2)	135.6 (64.8)	89.9 (67.2)
>24.9–29.9	260	45.6 (8.1)	134.7 (32.1)	35.4 (8.7)	193.6 (73.3)	176.0 (91.1)
>29.9–34.9	117	49.4 (10.2)	146.4 (36.3)	32.9 (9.7)	264.3 (83.0)	228.1 (100.2)
>35	54	50.7 (10.0)	147.8 (35.6)	29.2 (10.9)	398.4 (121.2)	269.1 (128.0)
<i>P</i> -value *		3.6×10 ⁻²²	7.1×10 ⁻¹⁹	2.3×10 ⁻¹²	1.0×10 ⁻²⁹	1.1×10 ⁻²⁹
Current smoking						
No	586	45.2 (10.1)	131.3 (35.1)	35.8 (9.8)	201.6 (105.6)	163.0 (109.4)
Yes	55	42.9 (8.6)	121.0 (29.9)	35.7 (11.1)	183.5 (112.6)	123.8 (88.4)

	PtNo.	SMI (cm ² /m ²)	Muscle area (cm ²)	Muscle attenuation (HU)	Subcutaneous fat area (cm ²)	Visceral fat area (cm ²)
<i>P</i> -value *		0.11	0.05	0.81	0.07	0.02
Cancer stage						
Local	213	45.3 (10.6)	130.7 (32.9)	34.6 (9.5)	217.5 (113.3)	170.7 (110.9)
Locally advanced	147	45.1 (9.9)	132.6 (35.6)	37.8 (10.3)	186.5 (103.3)	152.5 (99.6)
Metastatic	279	45.3 (9.7)	131.6 (36.0)	35.9 (9.5)	190.5 (98.6)	155.6 (106.3)
Unknown	48	43.5 (9.3)	126.9 (34.5)	35.2 (11.3)	241.0 (142.0)	176.0 (120.3)
<i>P</i> -value *		1.00	0.87	0.01	0.02	0.28
Primary tumor location						
Head/Uncinate	423	44.6 (10.2)	129.0 (33.8)	35.5 (10.1)	205.0 (110.7)	159.4 (105.6)
Body	131	45.0 (9.0)	130.6 (32.5)	36.9 (9.2)	185.8 (94.4)	155.9 (104.3)
Tail	78	46.5 (9.8)	137.0 (38.0)	34.5 (9.9)	213.9 (112.2)	177.9 (122.7)
<i>P</i> -value *		0.22	0.26	0.10	0.17	0.51

Body composition measurements reported as mean (standard deviation)

* Two-sided *P*-values calculated using Wilcoxon rank-sum test

Abbreviations: SMI, skeletal muscle index; HU, Hounsfield unit; BMI, body mass index

Extended Data Table 3

Hazard ratios (95% CI) for death among pancreatic cancer cases by body composition measurements on computed tomography (a) stratified by cancer stage at diagnosis and (b) overall.

a.	Pt. No.	Extreme Quintiles * ^{&}	Per S.D. *	P-interaction **
Visceral fat area (cm²)				0.59
Localized	213	2.02 (0.97–4.21)	1.15 (0.88–1.50)	
Locally advanced	147	0.53 (0.22–1.32)	0.81 (0.64–1.04)	
Metastatic	279	0.98 (0.54–1.76)	0.97 (0.80–1.17)	
Subcutaneous fat area (cm²)				0.72
Localized	213	1.29 (0.58–2.87)	1.44 (1.05–1.98)	
Locally advanced	146	0.64 (0.26–1.60)	0.83 (0.68–1.00)	
Metastatic	279	0.99 (0.54–1.80)	0.91 (0.73–1.12)	
SMI (cm²/m²)				0.90
Localized	210	0.66 (0.30–1.46)	0.84 (0.64–1.12)	
Locally advanced	145	0.59 (0.27–1.29)	0.87 (0.70–1.08)	
Metastatic	277	1.54 (0.85–2.79)	1.05 (0.84–1.30)	
Muscle area (cm²)				0.47
Localized	213	0.82 (0.34–1.98)	0.86 (0.62–1.19)	
Locally advanced	147	0.40 (0.16–1.00)	0.81 (0.62–1.06)	
Metastatic	279	1.56 (0.77–3.18)	1.10 (0.82–1.45)	
Muscle attenuation (HU)				0.49
Localized	210	0.32 (0.16–0.67)	0.74 (0.60–0.90)	
Locally advanced	147	0.99 (0.50–1.96)	0.94 (0.75–1.19)	

a.

	Pt. No.	Extreme Quintiles* ^{&}	Per S.D.*	P-interaction**
Metastatic	275	1.01 (0.60–1.69)	0.96 (0.80–1.16)	

b.

	Quintiles of Body Composition Measurements [@]					P-trend [§]
	1	2	3	4	5	
SMI (cm²/m²)						
Median OS (mo.)	11.1	11.0	10.8	11.6	11.7	
Hazard ratio (95% CI)***	1.0	0.98 (0.76–1.27)	1.04 (0.80–1.36)	0.92 (0.70–1.19)	0.91 (0.68–1.21)	0.35
Hazard ratio (95% CI)****	1.0	1.01 (0.78–1.31)	1.04 (0.79–1.37)	0.94 (0.71–1.24)	0.93 (0.68–1.27)	0.47
Muscle area (cm²)						
Median OS (mo.)	10.2	12.1	10.8	11.6	11.3	
Hazard ratio (95% CI)***	1.0	0.75 (0.58–0.98)	0.90 (0.69–1.17)	0.81 (0.62–1.05)	0.84 (0.63–1.12)	0.50
Hazard ratio (95% CI)****	1.0	0.78 (0.60–1.02)	0.91 (0.69–1.20)	0.82 (0.62–1.10)	0.87 (0.64–1.20)	0.71
Muscle attenuation (HU)						
Median OS (mo.)	10.2	11.2	10.8	12.7	11.7	
Hazard ratio (95% CI)***	1.0	0.89 (0.68–1.15)	0.92 (0.70–1.20)	0.75 (0.57–0.98)	0.87 (0.65–1.15)	0.16
Hazard ratio (95% CI)****	1.0	0.86 (0.65–1.13)	0.89 (0.67–1.18)	0.71 (0.53–0.96)	0.80 (0.57–1.11)	0.10

*Cox proportional hazards model adjusted for age at diagnosis (continuous), gender (male, female), race (white, non-white, unknown), year of diagnosis (2000–2005, 2006–2010, 2011–2015), institution (DF/BWCC, MGH, Mayo Clinic, Stanford University, UNC), BMI (continuous), diabetes history (none, 4yrs, >4yrs, unknown), and smoking status (never, past, current, unknown)

[&]Comparing top and bottom quintile

**Two-sided *P*-interaction calculated by Wald test of cross-product between body component measurement (continuous) and stage (local, locally advanced, metastatic, unknown)

[@]N=687 patients

***Cox proportional hazards model adjusted for age at diagnosis (continuous), gender (male, female), race (white, non-white, unknown), year of diagnosis (2000–2005, 2006–2010, 2011–2015), institution (DF/BWCC, MGH, Mayo Clinic, Stanford University, UNC), and cancer stage (local, locally advanced, metastatic, unknown)

****Cox proportional hazards model adjusted for age at diagnosis (continuous), gender (male, female), race (white, non-white, unknown), year of diagnosis (2000–2005, 2006–2010, 2011–2015), institution (DF/BWCC, MGH, Mayo Clinic, Stanford University, UNC), cancer stage (local, locally advanced, metastatic, unknown), BMI (continuous), diabetes history (none, 4yrs, >4yrs, unknown), and smoking status (never, past, current, unknown)

[§]Two-sided *P*-trend values calculated by entering quintile-specific median value for body composition measurements as continuous variable in Cox proportional hazards model

Abbreviations: CI, confidence interval; S.D., standard deviation; SMI, skeletal muscle index; HU, Hounsfield unit; DF/BWCC, Dana-Farber/Brigham and Women’s Cancer Center; MGH, Massachusetts General Hospital; UNC, University of North Carolina; BMI, body mass index

Extended Data Table 4

Plasma branched chain amino acid (BCAA) levels and clinical characteristics of pancreatic cancer cases.

	Pt No.	Total BCAAs (μM)
Age, years		
< 60	220	351.6 (174.9)
60 – <70	271	327.7 (104.3)
70	287	297.7 (84.8)
<i>P</i> -value *		1.3×10^{-6}
Gender		
Male	432	346.1 (101.2)
Female	346	295.0 (144.1)
<i>P</i> -value *		3.4×10^{-18}
Race		
White	696	322.2 (98.3)
Non-White	45	290.6 (122.2)
<i>P</i> -value *		0.10
Diabetes		
No diabetes	563	322.3 (129.0)
Diabetes 4 years	99	330.9 (113.8)
Diabetes >4 years	54	341.8 (122.7)
<i>P</i> -value *		0.24
Body-mass index, kg/m^2		
<18.5	14	286.3 (120.4)
18.5–24.9	245	316.7 (168.0)
>24.9–29.9	295	322.6 (91.5)
>29.9–34.9	131	337.0 (111.7)
>35	63	335.3 (99.0)
<i>P</i> -value *		0.01
Current smoking		
No	661	323.0 (101.2)
Yes	68	328.8 (291.0)
<i>P</i> -value *		0.04
Cancer stage		
Local	256	306.6 (89.0)
Locally advanced	155	321.1 (96.1)
Metastatic	308	332.9 (110.0)
Unknown	59	348.1 (283.8)
<i>P</i> -value *		0.05
Primary tumor location		
Head/Uncinate	479	311.7 (137.8)
Body	141	336.4 (107.1)

	Pt No.	Total BCAAs (μM)
Tail	96	345.5 (70.1)
<i>P</i> -value *		6.6×10^{-7}

Plasma BCAA measurements reported as mean (standard deviation)

* Two-sided *P*-values calculated using Wilcoxon rank-sum test

Abbreviations: BCAA, branched chain amino acids; μM , micromolar

Extended Data Table 5
 Pearson correlation coefficients for BCAAs, body composition measurements, and patient characteristics

Variable	BMI	Age at diagnosis	Valine	Leucine	Isoleucine	Total BCAA	SMI	Muscle area	Muscle attenuation	Subcutaneous fat area	Visceral fat area
BMI	1.00	-0.14*	0.10*	0.06	0.01	0.06	0.43**	0.38**	-0.30**	0.74**	0.58**
Age at diagnosis		1.00	-0.19**	-0.17**	-0.14*	-0.18**	-0.29**	-0.33**	-0.32**	-0.09*	0.03
Valine			1.00	0.92**	0.78**	0.95**	0.22**	0.29**	0.18**	0.03	0.18**
Leucine				1.00	0.91**	0.99**	0.17**	0.24**	0.17**	-0.01	0.12*
Isoleucine					1.00	0.93**	0.10*	0.14*	0.13*	-0.01	0.07
Total BCAA						1.00	0.17**	0.24**	0.17**	0.01	0.13*
SMI							1.00	0.84**	0.20**	0.15*	0.37**
Muscle area								1.00	0.23**	0.08*	0.44**
Muscle attenuation									1.00	-0.40**	-0.34**
Subcutaneous fat										1.00	0.43**
Visceral fat											1.00

N=687 patients

* Two-sided P < 0.05

** Two-sided P < 0.0001

Abbreviations: BCAA, branched chain amino acid; BMI, body mass index; SMI, skeletal muscle index

Extended Data Table 6

Hazard ratios (95% CI) for death among pancreatic cancer cases by plasma branched chain amino acids levels at diagnosis

	Quartiles of Plasma Branched Chain Amino Acids				<i>P</i> -trend*
	1	2	3	4	
Total BCAAs					
Median (μM)	217.7	284.3	343.3	425.0	
Range (μM)	72.9–255.7	255.8–312.8	312.9–374.3	374.5–2327.2	
Median OS (mo.)	10.6	10.8	12.4	12.1	
Hazard ratio (95% CI) **	1.00	0.95 (0.76–1.19)	0.79 (0.62–0.99)	0.81 (0.64–1.02)	0.04
Hazard ratio (95% CI) ***	1.00	0.96 (0.76–1.20)	0.78 (0.62–0.99)	0.82 (0.64–1.04)	0.06
Isoleucine					
Median (μM)	43.0	54.9	66.1	86.0	
Range (μM)	12.7–49.8	49.9–60.4	60.5–73.6	73.6–824.7	
Median OS (mo.)	10.8	11.7	11.6	11.6	
Hazard ratio (95% CI) **	1.0	0.89 (0.71–1.12)	0.93 (0.74–1.16)	0.89 (0.71–1.12)	0.42
Hazard ratio (95% CI) ***	1.0	0.89 (0.70–1.12)	0.90 (0.72–1.14)	0.90 (0.71–1.14)	0.49
Leucine					
Median (μM)	73.6	99.9	121.8	152.5	
Range (μM)	23.6–89.0	89.3–108.0	108.3–132.6	132.7–844.6	
Median OS (mo.)	10.6	11.1	12.1	11.9	
Hazard ratio (95% CI) **	1.0	0.91 (0.73–1.14)	0.81 (0.64–1.02)	0.82 (0.65–1.04)	0.08
Hazard ratio (95% CI) ***	1.0	0.93 (0.74–1.16)	0.82 (0.65–1.03)	0.84 (0.66–1.07)	0.12
Valine					
Median (μM)	98.6	129.0	155.5	191.3	
Range (μM)	35.4–114.0	114.2–141.9	142.0–171.3	171.4–658.0	
Median OS (mo.)	9.9	11.5	12.4	12.1	
Hazard ratio (95% CI) **	1.0	0.78 (0.62–0.99)	0.71 (0.56–0.90)	0.71 (0.56–0.91)	0.01
Hazard ratio (95% CI) ***	1.0	0.79 (0.62–1.00)	0.71 (0.56–0.90)	0.74 (0.57–0.94)	0.02

N=778 patients

* Two-sided *P*-trend calculated by entering quartile-specific median value for individual plasma BCAAs as continuous variable in Cox proportional hazards model

** Cox proportional hazards model adjusted for age at diagnosis (continuous), gender (male/female), race (white, non-white, unknown), year of diagnosis (2000–2005, 2006–2010, 2011–2015), institution (DF/BWCC, MGH, Mayo, Stanford, UNC), and cancer stage (local, locally advanced, metastatic, unknown)

*** Cox proportional hazards model additionally adjusted for BMI (continuous), diabetes history (none, 4yrs, >4yrs, unknown), and smoking status (never, past, current, unknown)

Abbreviations: CI, confidence interval; μM, micromolar; OS, overall survival; BCAAs, branched-chain amino acids; DF/BWCC, Dana-Farber/Brigham and Women's Cancer Center; MGH, Massachusetts General Hospital; UNC, University of North Carolina; BMI, body mass index

Supplementary Material

Refer to Web version on PubMed Central for supplementary material.

Acknowledgments

We thank members of the Vander Heiden and Wolpin labs for discussions and the Koch Institute Swanson Biotechnology Center, particularly the Animal Imaging and Preclinical Testing Facility, for technical assistance. Major funding for this work was provided by the Lustgarten Foundation to B.M.W. and M.G.V.H. L.V.D. was supported by NIH Ruth Kirschstein Fellowship (F32CA210421). A.B. was supported by P50CA127003 and the Robert T. and Judith B. Hale Fund for Pancreatic Cancer Research. A.M. was supported by F32CA213810. E.C.L. was supported by the Damon Runyon Cancer Research Foundation (DRG-2299-17). A.N.L. is a Robert Black Fellow of the Damon Runyon Cancer Research Foundation (DRG-2241-15). B.M.W. was supported by Robert T. and Judith B. Hale Fund for Pancreatic Cancer Research, NIH/NCI (U01CA210171), Department of Defense (CA130288), Pancreatic Cancer Action Network, Noble Effort Fund, Peter R. Leavitt Family Fund, Wexler Family Fund, and Promises for Purple. M.G.V.H. was supported in part by a Faculty Scholar grant from the Howard Hughes Medical Institute, and acknowledges additional funding from SU2C, The Ludwig Center at MIT, the Koch Institute Frontier Awards, the MIT Center for Precision Cancer Medicine, and the NIH (R01CA168653, P30CA14051).

References

1. Koppenol WH, Bounds PL, Dang CV. Otto Warburg's contributions to current concepts of cancer metabolism. *Nature reviews. Cancer*. 2011; 11:325–337. DOI: 10.1038/nrc3038 [PubMed: 21508971]
2. Petruzzelli M, Wagner EF. Mechanisms of metabolic dysfunction in cancer-associated cachexia. *Genes & development*. 2016; 30:489–501. [PubMed: 26944676]
3. Dewys WD, et al. Prognostic effect of weight loss prior to chemotherapy in cancer patients. Eastern Cooperative Oncology Group. *The American journal of medicine*. 1980; 69:491–497. [PubMed: 7424938]
4. Mueller TC, Bachmann J, Prokopchuk O, Friess H, Martignoni ME. Molecular pathways leading to loss of skeletal muscle mass in cancer cachexia--can findings from animal models be translated to humans? *BMC cancer*. 2016; 16:75. [PubMed: 26856534]
5. Fearon K, Arends J, Baracos V. Understanding the mechanisms and treatment options in cancer cachexia. *Nature Reviews Clinical Oncology*. 2013; 10:90–99. DOI: 10.1038/nrclinonc.2012.209
6. Penna F, et al. Anti-cytokine strategies for the treatment of cancer-related anorexia and cachexia. *Expert opinion on biological therapy*. 2010; 10:1241–1250. DOI: 10.1517/14712598.2010.503773 [PubMed: 20594117]
7. Flint TR, et al. Tumor-Induced IL-6 Reprograms Host Metabolism to Suppress Anti-tumor Immunity. *Cell metabolism*. 2016; 24:672–684. DOI: 10.1016/j.cmet.2016.10.010 [PubMed: 27829137]
8. Hingorani SR, et al. Preinvasive and invasive ductal pancreatic cancer and its early detection in the mouse. *Cancer cell*. 2003; 4:437–450. [PubMed: 14706336]
9. Mayers JR, et al. Elevation of circulating branched-chain amino acids is an early event in human pancreatic adenocarcinoma development. *Nature medicine*. 2014; 20:1193–1198. DOI: 10.1038/nm.3686
10. Agustsson T, et al. Mechanism of increased lipolysis in cancer cachexia. *Cancer research*. 2007; 67:5531–5537. DOI: 10.1158/0008-5472.CAN-06-4585 [PubMed: 17545636]
11. Michaelis KA, et al. Establishment and characterization of a novel murine model of pancreatic cancer cachexia. *J Cachexia Sarcopenia Muscle*. 2017
12. Ryden M, et al. Lipolysis--not inflammation, cell death, or lipogenesis--is involved in adipose tissue loss in cancer cachexia. *Cancer*. 2008; 113:1695–1704. DOI: 10.1002/cncr.23802 [PubMed: 18704987]
13. Shaw JH, Wolfe RR. Fatty acid and glycerol kinetics in septic patients and in patients with gastrointestinal cancer. The response to glucose infusion and parenteral feeding. *Ann Surg*. 1987; 205:368–376. [PubMed: 3105476]
14. Fearon K, et al. Definition and classification of cancer cachexia: an international consensus. *The Lancet. Oncology*. 2011; 12:489–495. DOI: 10.1016/s1470-2045(10)70218-7 [PubMed: 21296615]

15. Hwang RF, et al. Cancer-associated stromal fibroblasts promote pancreatic tumor progression. *Cancer research*. 2008; 68:918–926. DOI: 10.1158/0008-5472.can-07-5714 [PubMed: 18245495]
16. Herrington MK, Arnelo U, Permert J. On the role of islet amyloid polypeptide in glucose intolerance and anorexia of pancreatic cancer. *Pancreatology*. 2001; 1:267–274. DOI: 10.1159/000055822 [PubMed: 12120206]
17. Martin L, et al. Cancer cachexia in the age of obesity: skeletal muscle depletion is a powerful prognostic factor, independent of body mass index. *Journal of clinical oncology : official journal of the American Society of Clinical Oncology*. 2013; 31:1539–1547. DOI: 10.1200/jco.2012.45.2722 [PubMed: 23530101]
18. Mourtzakis M, et al. A practical and precise approach to quantification of body composition in cancer patients using computed tomography images acquired during routine care. *Applied physiology, nutrition, and metabolism = Physiologie appliquee, nutrition et metabolisme*. 2008; 33:997–1006. DOI: 10.1139/h08-075
19. Choi Y, et al. Skeletal Muscle Depletion Predicts the Prognosis of Patients with Advanced Pancreatic Cancer Undergoing Palliative Chemotherapy, Independent of Body Mass Index. *PLoS One*. 2015; 10:e0139749. [PubMed: 26437072]
20. Prado CM, et al. Prevalence and clinical implications of sarcopenic obesity in patients with solid tumours of the respiratory and gastrointestinal tracts: a population-based study. *The Lancet. Oncology*. 2008; 9:629–635. DOI: 10.1016/s1470-2045(08)70153-0 [PubMed: 18539529]
21. Rollins KE, et al. The impact of sarcopenia and myosteatosis on outcomes of unresectable pancreatic cancer or distal cholangiocarcinoma. *Clinical nutrition (Edinburgh, Scotland)*. 2016; 35:1103–1109. DOI: 10.1016/j.clnu.2015.08.005
22. Tan BH, Birdsell LA, Martin L, Baracos VE, Fearon KC. Sarcopenia in an overweight or obese patient is an adverse prognostic factor in pancreatic cancer. *Clinical cancer research : an official journal of the American Association for Cancer Research*. 2009; 15:6973–6979. DOI: 10.1158/1078-0432.ccr-09-1525 [PubMed: 19887488]
23. Vujasinovic M, Valente R, Del Chiaro M, Permert J, Lohr JM. Pancreatic Exocrine Insufficiency in Pancreatic Cancer. *Nutrients*. 2017; 9
24. Lv M, Zhu X, Wang H, Wang F, Guan W. Roles of caloric restriction, ketogenic diet and intermittent fasting during initiation, progression and metastasis of cancer in animal models: a systematic review and meta-analysis. *PloS one*. 2014; 9:e115147. [PubMed: 25502434]
25. Laquente B, et al. Supportive care in pancreatic ductal adenocarcinoma. *Clin Transl Oncol*. 2017
26. Apte M. Isolation of Quiescent Pancreatic Stellate Cells from Rat and Human Pancreas. *Pancreapedia: Exocrine Pancreas Knowledge Base*. 2011
27. Loftus SK, et al. Acinar cell apoptosis in Serpini2-deficient mice models pancreatic insufficiency. *PLoS genetics*. 2005; 1:e38. [PubMed: 16184191]
28. DiStefano MT, et al. The Lipid Droplet Protein Hypoxia-inducible Gene 2 Promotes Hepatic Triglyceride Deposition by Inhibiting Lipolysis. *The Journal of biological chemistry*. 2015; 290:15175–15184. DOI: 10.1074/jbc.M115.650184 [PubMed: 25922078]
29. Gabbi C, et al. Pancreatic exocrine insufficiency in LXRbeta^{-/-} mice is associated with a reduction in aquaporin-1 expression. *Proceedings of the National Academy of Sciences of the United States of America*. 2008; 105:15052–15057. DOI: 10.1073/pnas.0808097105 [PubMed: 18806227]
30. Kraus D, Yang Q, Kahn BB. Lipid Extraction from Mouse Feces. *Bio-protocol*. 2015; 5
31. Yuan C, et al. Survival among patients with pancreatic cancer and long-standing or recent-onset diabetes mellitus. *Journal of clinical oncology : official journal of the American Society of Clinical Oncology*. 2015; 33:29–35. [PubMed: 25403204]
32. Yuan C, et al. Prediagnostic body mass index and pancreatic cancer survival. *Journal of clinical oncology : official journal of the American Society of Clinical Oncology*. 2013; 31:4229–4234. DOI: 10.1200/jco.2013.51.7532 [PubMed: 24145341]
33. DerSimonian R, Laird N. Meta-analysis in clinical trials. *Controlled clinical trials*. 1986; 7:177–188. [PubMed: 3802833]

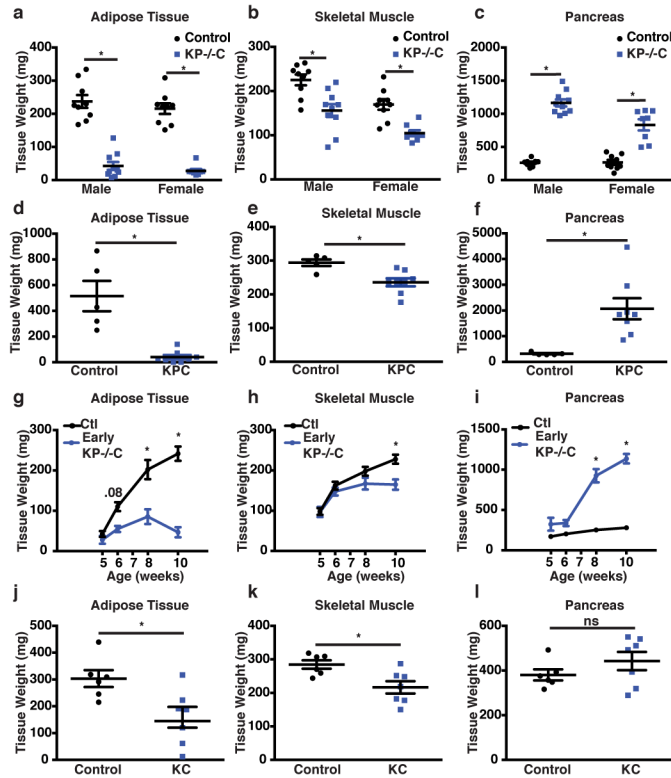


Figure 1. Early PDAC is associated with peripheral tissue wasting

a–c. Tissue weights of end-stage control and KP^{-/-}C mice (N= 9, 10 (males) and N= 9, 8 (females)). **a.** Epididymal AT (males) and inguinal subcutaneous AT weight (females) ($P < 1.25 \times 10^{-7}$). **b.** Gastrocnemius (GA) weight ($P = .002$ (males), $P = .0003$ (females)). **c.** Pancreas weight ($P < 1.16 \times 10^{-5}$). **d–f.** Tissue weights of end-stage male control and KPC mice (N=5, 8). **d.** Epididymal AT weight ($P = 0.0003$). **e.** GA weight ($P = 0.006$). **f.** Pancreas weight ($P = 0.007$). **g–i.** Peripheral tissue analysis during disease progression in control and KP^{-/-}C male mice (5wks, N=7, 5; 6wks, N=8, 7; 8wks, N=8, 10; 10wks, N= 10, 9). **g.** Epididymal AT mass (2-way ANOVA; 6wks, $P = 0.08$; 8wks, $P < 0.0001$; 10wks, $P < 0.0001$). **h.** GA weight (2-way ANOVA; 10wks, $P = 0.0007$). **i.** Pancreas weight (2-way ANOVA; 6wks, $P = 0.07$; 8wks, $P < 0.0001$; 10wks, $P < 0.0001$). **j–l.** Tissue weights of 15-week-old male control and KC mice (N=6). **j.** Epididymal AT weight ($P = 0.01$). **k.** GA weight ($P = 0.01$). **l.** Pancreas weight ($P = .23$). Unless otherwise indicated, statistical analysis was performed using unpaired two-sided *t*-test, data are mean \pm SEM, and N represents number of mice analyzed.

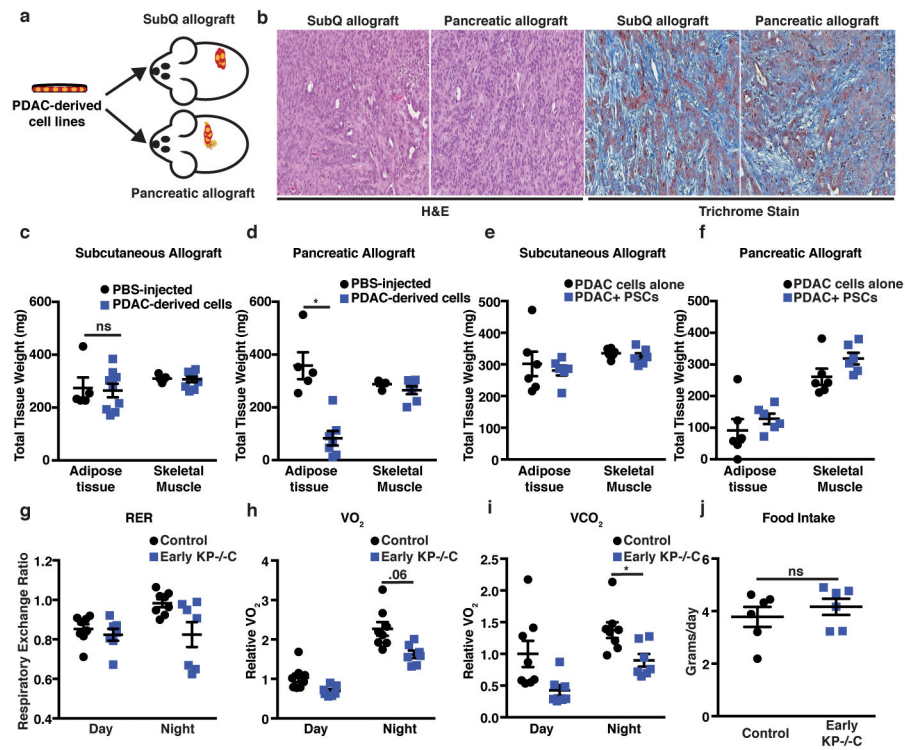


Figure 2. Pancreatic tumor growth promotes adipose tissue wasting

a. Schematic of experimental design. **b.** Representative H&E and Masson's trichrome histology of subcutaneous and orthotopic pancreatic tumors (N=4). **c–d.** Epididymal AT and GA muscle mass in mice injected with saline (PBS) or PDAC-cells. **c.** Mice bearing subcutaneous allografts (N=5, 9) ($P=.83$). **d.** Mice bearing pancreatic orthotopic allografts (N=5, 7) ($P<0.0001$). **e–f** Epididymal AT and GA mass in mice injected with PDAC cells or PDAC cells and PSCs. **e.** Mice bearing subcutaneous allograft tumors (N=6, 6) ($P=.63$). **f.** Mice bearing pancreatic allograft tumors (N=6, 6). **g–j** Metabolic cage measurements in male control and Early KP^{-/-}C mice (N=8, 7). **g.** Respiratory exchange ratio (RER). **h.** Relative volumetric oxygen consumption (VO₂) calculated from area under the curve measurements (AUC) for day and night ($P=.06$ (day) and $P=.129$ (night)). **i.** Relative volumetric carbon dioxide release (VCO₂) calculated from area under the curve measurements (AUC) for day and night ($P=.102$ (day) and $P=.01$ (night)). **j.** Food intake (g consumed/day) (N=6) ($P=.45$). Unless otherwise indicated, statistical analysis was performed using unpaired two-sided *t*-test, data are mean \pm SEM, and N represents number of mice analyzed.

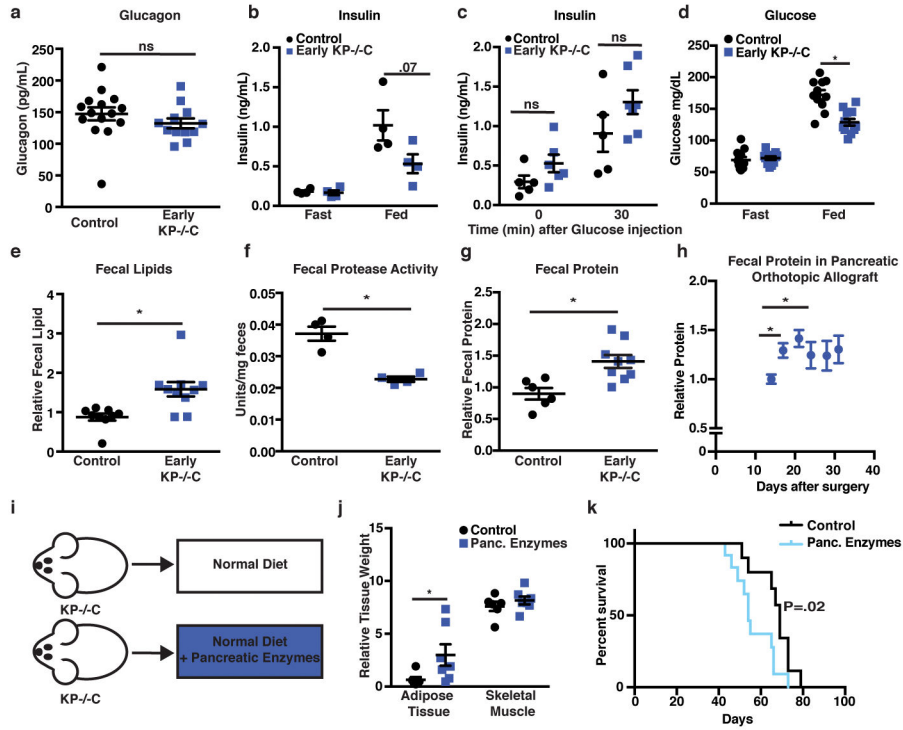


Figure 3. Decreased exocrine pancreatic function in early PDAC disease promotes tissue wasting
a–d. Endocrine function measurements in male control and early KP^{-/-}C mice. **a.** Fasted circulating glucagon levels (N=15, 12) (*P*=.28). **b.** Insulin levels in overnight fasted and fed mice (N=4). **c.** Insulin levels in mice before and after a glucose injection (N=5, 6) (*P*=.13 (Time=0), *P*=.16 (Time=30)). **d.** Glucose levels in overnight fasted and fed mice (N=11, 12) (*P*=.00008). **e–g.** Fecal analysis of male control and Early KP^{-/-}C mice. **e.** Total fecal lipid (N=9, 10) (*P*=.004). **f.** Total fecal protease activity (N=4) (*P*=.0009). **g.** Total fecal protein level (N=6, 9) (*P*=.004). **h.** Total fecal protein levels over time in male C57Bl/6J mice following orthotopic implantation of PDAC cells into the pancreas (N=5) (*P*=.008 (Day 14 vs Day 17), *P*=.005 (Day 14 vs Day 21)). **i.** Schematic of experimental design. **j.** Relative weights of KP^{-/-}C male mice fed a control diet or a diet supplemented with pancreatic enzymes (N=6, 7) (*P*=.033). **k.** Survival of male KP^{-/-}C mice fed the indicated diet (N=12) (Mantel-Cox test, *P*=.02). Unless otherwise indicated, statistical analysis was performed using unpaired two-sided *t*-test, data are mean ± SEM, and N represents number of mice analyzed.

Hazard ratios (95% CI) for death among pancreatic cancer cases by body composition measurements on computed tomography (CT) imaging

Table 1

	Quintiles of Body Composition Areas					P-trend [§]
	1	2	3	4	5	
Visceral adipose tissue area						
No. of cases	136	138	138	138	137	
Median (cm ²)	34.7	108.2	171.0	228.9	312.0	
Median OS (mo.)	12.3	10.2	11.5	11.3	11.1	
Hazard ratio (95% CI) *	1.0	1.25 (0.96–1.62)	1.06 (0.82–1.38)	1.08 (0.83–1.41)	1.04 (0.79–1.36)	0.73
Hazard ratio (95% CI) **	1.0	1.33 (1.01–1.74)	1.10 (0.82–1.47)	1.14 (0.84–1.56)	1.16 (0.82–1.63)	0.31
Subcutaneous adipose tissue area						
No. of cases	136	138	137	138	137	
Median (cm ²)	82.7	136.9	177.5	234.7	351.0	
Median OS (mo.)	11.9	10.6	12.0	11.6	10.2	
Hazard ratio (95% CI) *	1.0	1.18 (0.91–1.53)	0.97 (0.75–1.26)	0.92 (0.71–1.19)	1.06 (0.81–1.38)	0.80
Hazard ratio (95% CI) **	1.0	1.19 (0.91–1.57)	0.99 (0.74–1.32)	1.04 (0.77–1.41)	1.25 (0.86–1.82)	0.44
Sarcopenia[‡]						
	No	Yes	P-value			
No. of cases [#]	248	462				
Median OS (mo.)	11.6	11.3				
Hazard ratio (95% CI) *	1.0	1.03 (0.86–1.24)	0.74			
Hazard ratio (95% CI) **	1.0	1.04 (0.85–1.27)	0.72			
Sarcopenic Obesity						
Sarcopenia	No	No	Yes	Yes	Yes	
Obesity	No	Yes	No	Yes	Yes	
No. of cases [‡]	54	186	191	262	262	
Median OS (mo.)	11.1	12.0	10.4	11.9	11.9	
Hazard ratio (95% CI) *	1.0	0.98 (0.69–1.38)	1.11 (0.79–1.57)	0.95 (0.67–1.33)	0.95 (0.67–1.33)	

	Quintiles of Body Composition Areas					P-trend [§]
	1	2	3	4	5	
Hazard ratio (95% CI) ^{**}	1.0	0.90 (0.60–1.35)	1.12 (0.80–1.58)	0.91 (0.63–1.32)		

* Cox proportional hazards model adjusted for age at diagnosis (continuous), gender (male, female), race (white, non-white, unknown), year of diagnosis (2000–2005, 2006–2010, 2011–2015), institution (DF/BWCC, MGH, Mayo Clinic, Stanford University, UNC), and cancer stage (local, locally advanced, metastatic, unknown)

** Cox proportional hazards model additionally adjusted for BMI (continuous), diabetes history (none, 4yrs, >4yrs, unknown), and smoking status (never, past, current, unknown)

Eight patients were excluded due to missing information on height.

[†] A further 17 patients were excluded due to missing information on weight

[‡] Sarcopenia is defined as skeletal muscle index (SMI; ratio of skeletal muscle area [cm²] to height squared [m²]) <55.4 cm²/m² for men, and SMI <38.9 cm²/m² for women measured on baseline computed tomography imaging. Obesity is defined as body mass index (BMI) >25 kg/m².

[§] Two-sided P-trend is calculated by entering quintile-specific median value for adipose tissue area as continuous variable in Cox proportional hazards model.

Abbreviations: CI, confidence interval; OS, overall survival; DF/BWCC, Dana-Farber/Brigham and Women’s Cancer Center; MGH, Massachusetts General Hospital; UNC, University of North Carolina